Nanoscale

ROYAL SOCIETY OF CHEMISTRY

ARTICLE

Two-Dimensional Boron-Nitrogen-Carbon Monolayers with Tunable Direct Band Gaps

Miao Zhang[a, b, †], Guoying Gao[c, †], Alex Kutana[c], Yanchao Wang[a], Xiaolong Zou[c], John S. Tse[d], Boris I. Yakobson[c,*], Hongdong Li[a,*], Hanyu Liu[a,d,*], and Yanming Ma[a]

The search for new candidate semiconductors with direct band gaps of ~1.4 eV has attracted significant attention, especially among the two-dimensional (2D) materials, which have become potential candidates for next-generation optoelectronics. Here, we systematically studied 2D $B_{x/2}N_{x/2}C_{1-x}$ ($0<x<1$) compounds, and in particular focus on four stoichiometric $B_{x/2}N_{x/2}C_{1-x}$ (x=2/3, 1/2, 2/5 and 1/3) by using a recently developed global optimization method (CALYPSO) in conjunction with density functional theory. Furthermore, we examine more stoichiometries by the cluster expansion technique based on a hexagonal lattice. The results reveal that all monolayer $B_{x/2}N_{x/2}C_{1-x}$ stoichiometries adopt planar honeycomb character and are dynamically stable. Remarkably, electronic structural calculations show that most of $B_{x/2}N_{x/2}C_{1-x}$ phases possess direct band gaps within the optical range, thereby they can potentially be used in high-efficiency conversion of solar energy to electric power, as well as in p-n junction photovoltaic modules. The present results also show that band gaps of $B_{x/2}N_{x/2}C_{1-x}$ can be widely tuned within the optical range by changing the concentration of carbon that allows fast development of band gap-engineered materials in optoelectronics. These new findings may enable new approaches to design of microelectronic devices.

1. Introduction

In recent years, large demand of society for new clean energy and the shortcomings of the current silicon solar cells call for the exploration of new materials, which can make full use of the solar spectrum and possess better optoelectronic properties. Graphene, a zero-gap semi-metal with unique electronic properties,[1-3] is attractive for demonstrating fundamental physics in materials and potential applications in next-generation electronics. However, zero-gap nature of graphene prevents its use in optoelectronic applications. Monolayer MoS_2 was found to have a direct band gap and can be used to construct interband tunnel field-effect transistors, which have lower power consumption than classical transistors.[4, 5] However, monolayer MoS_2 is usually unstable and easily oxidized under normal conditions. So far, bulk silicon (Si), with a direct gap (~3.4 eV)[6] and indirect gap of ~1.1 eV, is still the leading material in the current solar cell markets.

However, Si is not optimal for optoelectronic applications because of its low conversion efficiency due to the indirect band gap.

Recently, Kim *et al.*[7] synthesized an orthorhombic silicon allotrope (Si_{24}) with a quasidirect band gap of ~1.3 eV via a chemical process where a Na_4Si_{24} precursor was synthesized at high pressure. Meanwhile, a series of Si allotropes[8-11] with quasidirect band gaps have been proposed theoretically. However, there is still a lack of materials with direct band gaps around the optimal value of ~1.4 eV[12] for the solar converting efficiency. This raises an important question: is it possible to design a new two-dimensional direct band gap semiconductor with an optimal gap value? Considering the zero-gap electronic structure of graphene and the large band gap of insulating single-layer *h*-BN and its ribbons,[13,14] it may be feasible to combine both, due to the similarity of lattice parameters and atomic arrangements, to get direct band gap materials with any desirable value. Indeed, Ci *et al.*[15] have reported a systematic route of co-depositing graphene and BN domains to synthesize large-area atomic layers of *h*-BNC material, which consists of hybridized, randomly distributed domains of BN and graphene phases. Later, same workers[16] and another group[17] reported a topological substitution reaction that converts graphene to *h*-BNC and then *h*-BN layers. These boron-nitrogen-carbon domains exhibit their structural features and band gaps distinct from pure BN and graphene and thus may possess excellent electronic properties, with potential for application in optoelectronic industry. It is noted that a previous theoretical work systematically studied half-

a. State Key Laboratory of Superhard Materials, Jilin University, Changchun 130012, China
b. College of Physics, Beihua University, Jilin 132013, China
c. Material Science and Nanoengineering, Rice University, Houston, 77005, USA
d. Department of Physics and Engineering Physics, University of Saskatchewan, Saskatoon, Saskatchewan S7N 5E2, Canada
e.

† M. Zhang and G. Gao contributed equally to this work. * Correspondence and requests for materials should be addressed to B. Yakobson (biy@rice.edu), H. Li (hdli@jlu.edu.cn), H. Liu (lhy@calypso.cn).
Electronic Supplementary Information (ESI) available: [details of any supplementary information available should be included here]. See DOI: 10.1039/C5NR03344F

metallicity in hybrid BCN nanoribbons by performing first-principles electronic-structure calculations.[18] Their results suggest the BNC nanoribbons may be considered as potential spintronic devices.[18] There is a theoretical study on BNC_2 nanoribbon, which shows a rich variety of electronic and magnetic properties.[19] Theoretical works[20, 21]["Consistent Methodology for Calculating Surface and Interface Energies", K. Rapcewicz, B. Chen, B. Yakobson, J. Bernholc, Phys. Rev. B 57, 7281-7291 (1998)] show that BN-graphene domains prefer a triangle shape in large scale, which is also observed in experiment.[17] However, there is still no systematic theoretical or experimental study on 2D $B_{x/2}N_{x/2}C_{1-x}$ when the size of the geometry goes to a few angstroms. Therefore, the investigation of 2D $B_{x/2}N_{x/2}C_{1-x}$ monolayer is required.

In this work, we have systematically explored structures of 2D $B_{x/2}N_{x/2}C_{1-x}$ "alloy" monolayers using the particle swarm optimization (PSO) technique[22, 23] as well as the cluster expansion (CE) method.[24] After establishing the hexagonal lattice type in $B_{x/2}N_{x/2}C_{1-x}$ by CALYPSO, we investigate these stoichiometries with the CE method on a hexagonal lattice. Both methods confirm the thermodynamic immiscibility of BN and C in $B_{x/2}N_{x/2}C_{1-x}$. Our analytical results based on the triangle geometry further support that 2D $B_{x/2}N_{x/2}C_{1-x}$ tends to phase separate. Interestingly, the calculated electronic properties show that 2D BNC, BNC_2, and BNC_3 monolayers possess direct band gaps of 1.56, 1.60, and 1.04 eV, respectively, which are within the favorable optical range. Our extended study also shows that other metastable stoichiometries have also direct band gaps and the values can be tuned by changing the concentration of carbon or BN. Our current results indicate that these novel materials could be promising candidates for microelectronic devices.
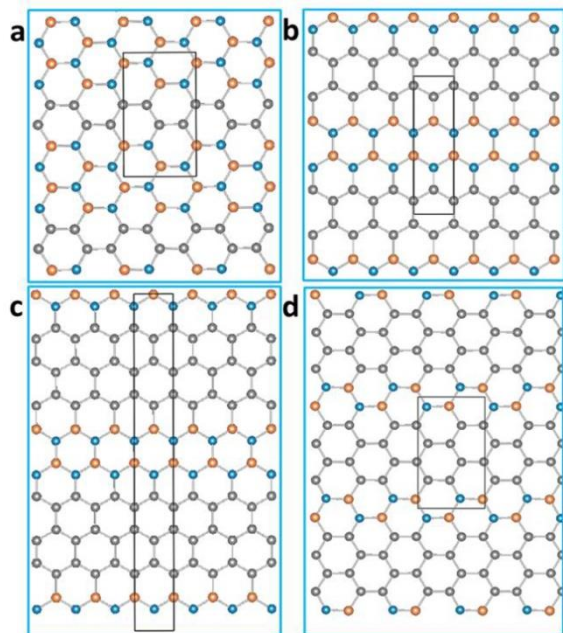

Figure 1. Predicted metastable $(BN)_{x/2}C_{1-x}$ structures. Four structures for (**a**) BNC, (**b**) BNC_2, (**c**) BNC_3, and (**d**) BNC_4 predicted with CALYPSO. B, C, and N atoms are denoted by orange, grey, and blue circles, respectively.

2. RESULTS

2D structures and formation energy. Four different compositions of 2D $B_{x/2}N_{x/2}C_{1-x}$ (x = 2/3, 1/2, 2/5 and 1/3) are first considered using CALYPSO. The results show that the most stable structure for each stoichiometry has the planar honeycomb feature (Figure 1). Figure 1a shows the stable structure of BNC monolayer, which can be seen as isolated 1D armchair carbon chains embedded into an h-BN monolayer. This planar honeycomb structure character shows clear trend of phase separation into graphene and h-BN.
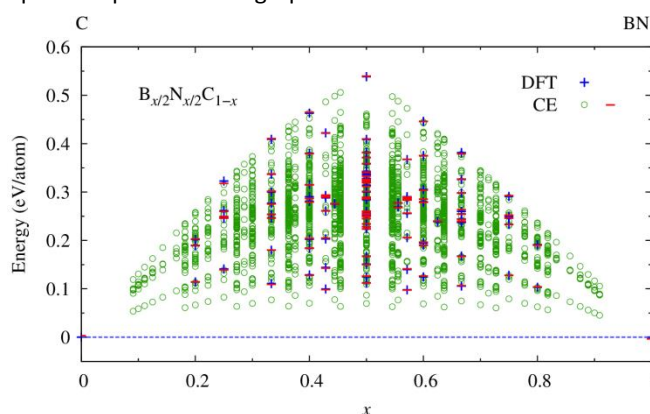

Figure 2. Formation energy of predicted $B_{x/2}N_{x/2}C_{1-x}$. Mixing energies of two-dimensional boron-nitrogen-carbon compounds $B_{x/2}N_{x/2}C_{1-x}$ as a function of concentration x obtained from the DFT and cluster expansion method. Blue crosses mark the DFT results, while green circles show the cluster expansion fitting. Red horizontal dashes show fitted values corresponding to those obtained with DFT. The reference energies are graphene and 2D h-BN.

The C-C bond lengths in BNC are 1.41 and 1.43 Å, which are similar to those in graphene (1.42 Å). The B-N bond lengths are 1.44, 1.45, and 1.46 Å, which are also close to those of 1.45 Å in h-BN. The similarity of C-C and B-N bond lengths in BNC to those in graphene and h-BN further supports the phase separation. The structure of 2D BNC_2 is composed of 1-D chain edge-shared hexagonal carbon and BN, which also shows the trend of phase separation. The C-C and B-N bond lengths in BNC_2 are also similar to those in graphene and BN. As the concentration of carbon increases continuously, the inclusions of graphene become much more evident in BNC_3. It is clearly seen that the BNC_4 monolayer (Figure 1d) consists of an armchair chain of B and N atoms and a large width of graphene. It is worth noting that the ordering of the bond strength follows the sequence: B–N (4.00 eV) > C–C (3.71 eV) > C–N (2.83 eV) > B–C (2.59 eV) > B–B (2.32 eV) > N–N (2.11 eV).[25] All structures maximize the number of stable bonds, such as B–N and C–C bonds, which further support the phase separation. In overall, all of the four stoichiometries show the phase separation trend with the common planar honeycomb structural character. This strongly suggests other stoichiometric $B_{x/2}N_{x/2}C_{1-x}$ may also adopt honeycomb structure motif. Therefore, we proceed to examine the energetics of $B_{x/2}N_{x/2}C_{1-x}$ with the CE[24] method based on the honeycomb lattice, which allows us to easily investigate the structures with larger unit cell. Figure 2 shows the computed formation energies of honeycomb 2D $B_{x/2}N_{x/2}C_{1-x}$ obtained with

DFT and from the fitted CE Hamiltonian. As expected, mixing energies are positive, indicating phase separation into graphene and BN. While thermodynamically just metastable, some of the phases show remarkable dynamic stability in high-temperature MD calculations,[26] which will be discussed later, and thus may indeed be regarded as metastable materials. We have also calculated the formation energy of $B_{x/2}N_{x/2}C_{1-x}$ (x=2/3, 1/2, 2/5 and 1/3) with respect to 2D boron, graphene, and N_2 molecule, following previous work on boron-carbon fullerenes, which shows the tendency of boron to form patches. [28] Our results indicate that boron-nitrogen-carbon system is stable relative to 2D boron [Penev *et al*. Nano let. **12**, 2441 (2012)],[27] graphene and N_2 molecule. Although boron-nitrogen-carbon system is metastable compared to graphene and *h*-BN, suitable substrates might stabilize some of the proposed structures.

It has been established in previous theoretical works that graphene or BN domains prefer a triangular shape at large scale.[20, 21] It is thus necessary for us to consider the triangular and other geometries (here is nanoribbon) for different stoichiometries using the analytical method. The formation energies for the four predicted structures obtained from the analytical model are very close to those calculated by the DFT method, supporting the reliability of these analytical results (see Figure 3). The formation energies are always above the energies of graphene and *h*-BN, again supporting the immiscibility proposed above. The analytical results show that the formation energy will decrease as the triangle size or nanoribbon width of graphene or BN increases, reflecting the fact that larger structures are closer to full phase separation than smaller ones at all stoichiometries, which is in agreement with experimental observations.
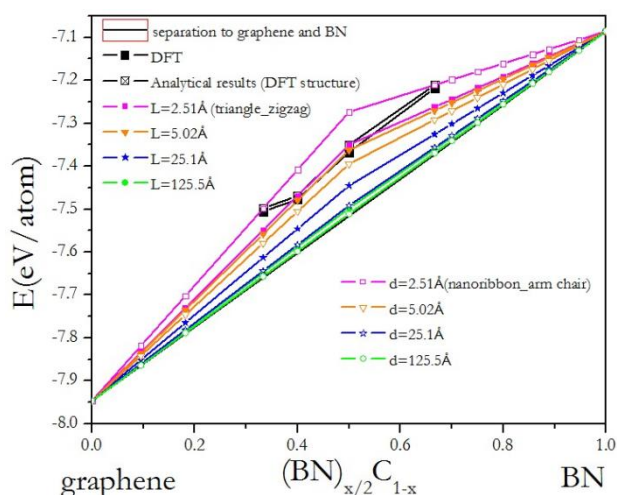

Figure 3. Formation energies of $(BN)_{x/2}C_{1-x}$ sheets as a function of *x* calculated with DFT and obtained from analytical expressions. Straight black line connects formation energy of graphene and *h*-BN, respectively. The solid black squares correspond to the calculated DFT data for the predicted structures, while the hollow black squares show the analytical results for the predicted structures. Other solid and hollow symbols show the analytical results for the assumed zigzag triangle and armchair nanoribbon geometries, respectively. Different triangle sizes (*L*) and armchair widths (*d*) are indicated in the figure.

Electronic structures. It is well known that graphene is a zero band-gap semi-metal, while 2D hexagonal boron nitride is a representative insulator with a band gap of ~6 eV.[29] Therefore, it is expected that the band gap of $B_{x/2}N_{x/2}C_{1-x}$ will be smaller than that of 2D *h*-BN. Using the PBE functional, BNC is calculated to be a semiconductor with a band gap of 1.05 eV, as can be seen from the calculated band structure shown in Figure 4a. It is well known that the screened hybrid functional of Heyd, Scuseria, and Ernzerhof (HSE)[30] usually gives more accurate electronic band gaps than that of PBE functional. Using the HSE functional, the calculated band gap is 1.56 eV
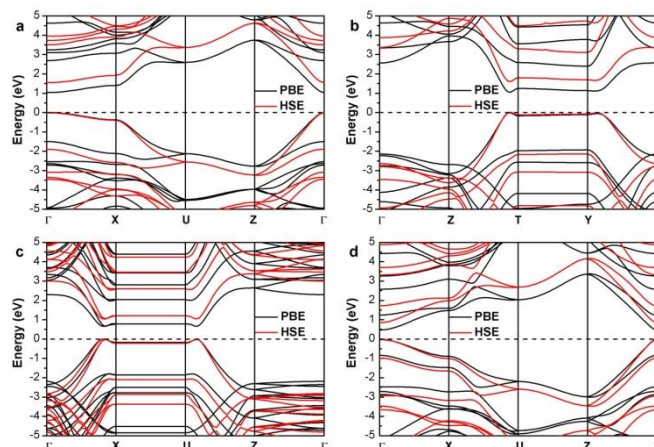

Figure 4. Electronic properties of predicted BNC_x structures. Calculated band structures of (a) BNC, (b) BNC_2, (c) BNC_3, and (d) BNC_4 using PBE (black line) and HSE (red line) functional, respectively.

for BNC. Similarly, BNC_2 and BNC_3 (Figure 4b and c) are calculated to have band gaps of 1.6 and 1.04 eV with HSE functional (1.06 and 0.67 eV with PBE functional), respectively. BNC_4 has a much smaller band gap of 0.86 eV (HSE) (0.49 eV, PBE), which is understandable considering its much higher concentration of carbon. Both the valence band maximum (VBM) and the conduction band minimum (CBM) of each band structure are located at the same k-point such as the Brillouin zone center for BNC and BNC_4, which suggests that they have direct band gaps. The band gaps for $B_{x/2}N_{x/2}C_{1-x}$ (x=2/3, 1/2 and 2/5) range from 1.04 eV to 1.6 eV, which is close to the onset of the visible spectrum. Based on these results, we extend our study to other stoichiometries. Band gap variations for more $B_{x/2}N_{x/2}C_{1-x}$ stoichiometries are shown in Figure 5. Due to the great disparity of the band gaps of graphene and *h*-BN, one can potentially achieve great gap variability in the mixture. The computed results present the possibility of gap tuning over a wide range of values, which is much better than the earlier results for 2D transition metal dichalcogenide alloys $Mo_{1-x}W_xS_2$ and $MoSe_{2(1-x)}S_{2x}$.[31]

According to the Shockley-Queisser limit, the maximum theoretical solar conversion efficiency of a single p-n junction cell is a function of the band gap of materials, with a maximum of 33.7% solar energy that can be employed near a band gap of 1.34 eV.[32] However, the current commercial silicon cells can only reach the efficiency of 15-20%,[33] due to the large difference in the converting efficiency between direct and indirect gap materials. Interestingly, the calculated band-gap

values for $B_{x/2}N_{x/2}C_{1-x}$ (x = 2/3, 1/2 and 2/5) fall into the optimum range. Thus it is probably that the predicted 2D $B_{x/2}N_{x/2}C_{1-x}$ structures are potentially suitable for multiple p–n junction photovoltaic modules.
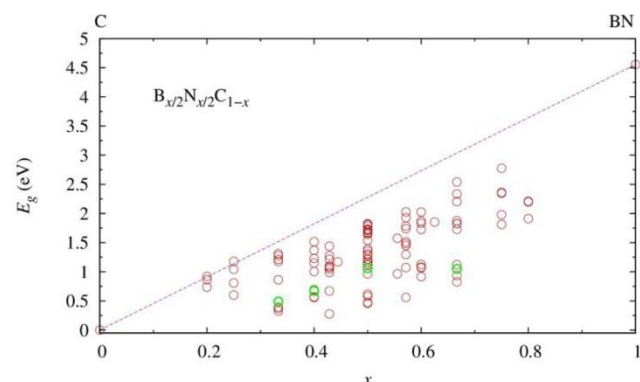

Figure 5. Calculated band gaps of 2D boron-nitrogen-carbon compounds $B_{x/2}N_{x/2}C_{1-x}$. The four green circles are the calculated ones by PBE for the four structures predicted by CALYPSO.

Structural stability. To investigate the dynamical stability of $B_{x/2}N_{x/2}C_{1-x}$ monolayers, we computed phonon dispersions for the predicted structures. As shown in Figure S2, no imaginary phonon modes are present, indicating that all predicted 2D $B_{x/2}N_{x/2}C_{1-x}$ structures are dynamically stable. We have also performed first-principles molecular dynamics (MD) simulations to examine the thermal stability of 2D structures using the canonical *NVT* (*N*- number of particles, *V*-Volume and *T*-temperature) ensemble. Supercells of 2 × 3 × 1, 5 × 2 × 1, 5 × 1 × 1, and 2 × 3 × 1 were used for BNC, BNC_2, BNC_3, and BNC_4, respectively. For each stoichiometry, MD calculations were performed at temperatures of 300, 1000, 1500, and 2000 K. Each simulation consists of 10000 time steps with a time step of 1 fs. The results show that monolayer BNC_4 is thermally stable at least up to 1000 K, while monolayer BNC, BNC_2, and BNC_3 can maintain their structural integrity even up to 2000 K.

3. DISCUSSION

It is well known that sunlight can be directly converted into electricity in solar cells. The absorption range of the energy of sunlight is from ~1.13 eV to ~4.13 eV. A perfect candidate for optoelectronic applications should possess a direct band gap and the absorption band should also be commensurate with the visible region. It is encouraging that all the predicted $B_{x/2}N_{x/2}C_{1-x}$ monolayers are with direct band gaps and their band-gap values can be tuned to any desirable value by adjusting the concentration of carbon or BN. This property is suitable for donor materials for solar cells optoelectronic applications. To evaluate the optical absorption, we employed the HSE functional to calculate the absorption spectra (the imaginary part of the dielectric functions ε). The calculated results are shown in Figure 6.

According to the reference of air mass (AM) 1.5 solar spectral irradiance, the solar spectrum has the maximum intensity in

the visible light range. It can be seen that the optical absorption spectra of BNC and BNC_2 monolayers are located within the visible light range. For BNC and BNC_2 monolayer, the maximum peak of the absorption band (~2.26 and ~2.25 eV) locates within yellow light range. In comparison, the maximum absorption band of BNC_3 (~1.58 eV) is located in the red range, while that of BNC_4 monolayer (~1.49 eV) is in the infrared light range. The theoretical results reveal that the four 2D $B_{x/2}N_{x/2}C_{1-x}$ stoichiometries may be promising candidates for nanoscale solar cell absorbers.
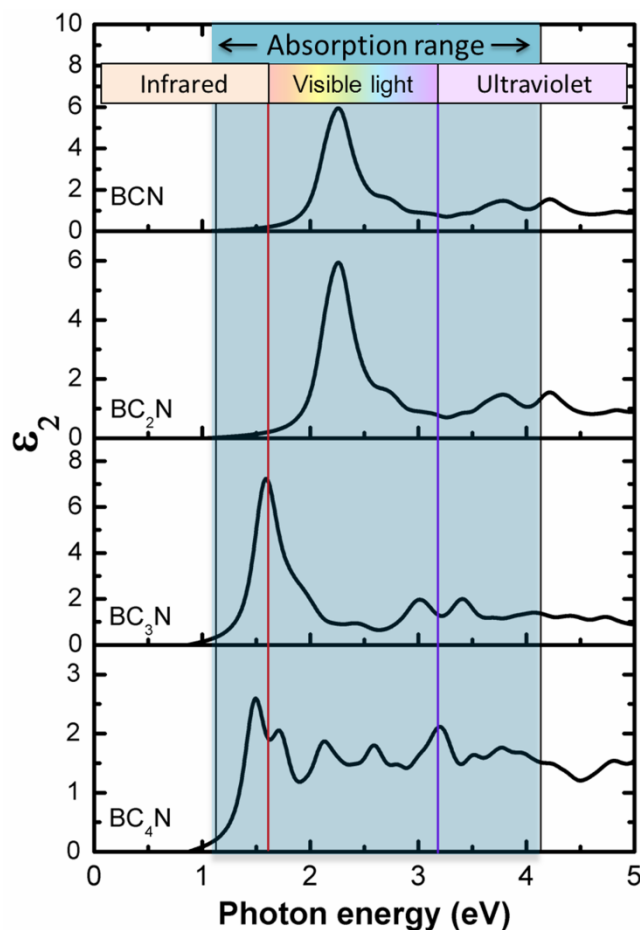

Figure 6. Optical properties of predicted $B_{x/2}N_{x/2}C_{1-x}$ structures. Imaginary part of the dielectric functions (ε^2) within the HSE functional for BCN, BC_2N, BC_3N and BC_4N monolayer structures. The vertical red and blue color lines represent the energy of red and blue edges of the visible spectrum.

4. METHODS

CALYPSO method for 2D system. For structure search we employed the swarm intelligence based CALYPSO method and its same name code,[22, 23] which was unbiased against prior known structures. The method has been demonstrated to correctly predict crystal structures of a diverse variety of materials.[11, 34-38] In this study, we considered four compositions in structure searches, *viz*. BNC, BNC_2, BNC_3, and BNC_4. The population size is 50 and the number of generations is 50. Various supercell sizes are considered with up to 4 formula units. Initial random structures were constructed by generating atomic coordinates using crystallographic

symmetry operations. The candidate structures are then fully optimized using the standard density functional theory (DFT) method. 60% of the best structures are selected through PSO to generate the next generation, while other structures are generated randomly to guarantee the structure diversity.

Calculation details. DFT method is used for structural relaxation and electronic structure calculation. The ion–electron interaction is treated by the projector augmented-wave[39, 40] technique, which is performed in the Vienna *ab initio* simulation package.[41] In the DFT plane-wave calculations, we use the Perdew–Burke–Ernzerhof [42] generalized gradient approximation. The 2D k-mesh was generated by the Monkhorst–Pack scheme and the density depends on the lattice constant. For each structure, the relaxation is considered to converge when the atomic forces are less than 0.001 eV/Å. A vacuum distance of ~15 Å is used so that the interlayer interaction is negligible. Since the semi-local DFT PBE functional is known to underestimate the band gap of predicted structures, HSE functional[30, 43] including exact exchange was used to calculate the electronic and optical properties. To investigate the dynamical stability, we employed the finite displacement method as implemented in the PHONOPY code[44] to calculate the phonon band structure.

Analytical results: For $(BN)_xC_{1-x}$ mixing with fractions x of BN and 1-x of graphene, we also obtained the formation energy by analytical formula by taking the experimental observed triangle-shape BN in graphene ($x \leq 0.5$) or graphene in BN ($x \geq 0.5$) with zigzag interface. For simplicity, we considered two triangles (one is just the inversion of the other). For the triangle-shaped BN in graphene, it is either B-rich or N-rich. Here, the triangle is of size of L and L is in units of l, (l is 2.46 and 2.51 Å in graphene and BN, respectively), one can estimate formation energy by the expression:

$$\varepsilon_{(BN)_{\frac{x}{2}}C_{1-x}} = (1-x)\varepsilon_C + x\varepsilon_{BN} - \left(\frac{3L\Gamma_{ZB}}{N_t} + \frac{3L\Gamma_{ZN}}{N_t}\right) = (1-x)\varepsilon_C + x\varepsilon_{BN} - \frac{3L\Gamma_Z}{N_t}$$

(1)

Here, ε_C and ε_{BN} are the formation energies for pure graphene and pure BN (ε_C =-7.947eV/atom, ε_{BN} =-7.086eV/atom). The BN/C interface energies Γ_A and Γ_Z are 0.2231 and 0.52988 eV/Å, respectively, which are taken from our previous paper.[16]

When $x \leq 0.5$, i.e., for BN isles in graphene:

$$\varepsilon_{(BN)_{\frac{x}{2}}C_{1-x}} = (1-x)\varepsilon_C + x\varepsilon_{BN} - \frac{3L\Gamma_Z}{N_t} = (1-x)\varepsilon_C + x\varepsilon_{BN} - \frac{3\Gamma_Z x}{2 \times \left(\frac{L}{l^2} + \frac{4}{l} + \frac{1}{L}\right)}$$

(2)

When $x \geq 0.5$, i.e., for graphene isles in BN:

$$\varepsilon_{(BN)_{\frac{x}{2}}C_{1-x}} = (1-x)\varepsilon_C + x\varepsilon_{BN} - \frac{3L\Gamma_Z}{N_t} = (1-x)\varepsilon_C + x\varepsilon_{BN} - \frac{3\Gamma_Z (1-x)}{2 \times \left(\frac{L}{l^2} + \frac{4}{l} + \frac{1}{L}\right)}$$

(3)

We also obtain the formation energy for the predicted structures by analytical formula.

Both structures in Figures 1a and 1d have armchair interface, so the formation energy is

$$\varepsilon_{(BN)_{\frac{x}{2}}C_{1-x}} = (1-x)\varepsilon_C + x\varepsilon_{BN} - \frac{2mL\Gamma_A}{N_t}$$ or

$$\varepsilon_{(BN)_{\frac{x}{2}}C_{1-x}} = (1-x)\varepsilon_C + x\varepsilon_{BN} - \frac{\sqrt{3}l^2\Gamma_A}{2} \times \frac{x}{d}$$

(4)

Both structures in Figure 1b and 1c have zigzag interface, so the formation energy is

$$\varepsilon_{(BN)_{\frac{x}{2}}C_{1-x}} = (1-x)\varepsilon_C + x\varepsilon_{BN} - \frac{mL\Gamma_Z}{N_t}$$ or

$$\varepsilon_{(BN)_{\frac{x}{2}}C_{1-x}} = (1-x)\varepsilon_C + x\varepsilon_{BN} - \frac{\sqrt{3}l^2\Gamma_Z}{4}\frac{x}{d}$$

(5)

Here, m is the total number of carbon or BN ribbons in each primitive cell. N_t is the total number of atoms in each primitive cell, L is the length of the primitive cell parallel to the carbon or BN chain, which can be armchair or zigzag, and d is the width of carbon or BN.

In the CE formalism, mixing energies of compounds are fitted by a multivariate polynomial expansion in discrete variables describing site occupancies of a lattice. The resulting Hamiltonian is presented in a compact form as a sum of n-tuple clusters of lattice sites. This permits fast evaluation of mixing energies for different atomic configurations. The CE fitting of the mixing energies computed with DFT was carried out with the Alloy-Theoretic Automated Toolkit (ATAT) code.[45] A total of 106 $B_{x/2}N_{x/2}C_{1-x}$ structures were used in the fitting procedure. The root-mean-square deviation of the CE-fitted mixing energies from the actual values (the cross-validation score) was 3 meV/atom, indicating a good fit.

5. CONCLUSION

In conclusion, we have performed a global search of the crystal structures of 2D $B_{x/2}N_{x/2}C_{1-x}$ (x=2/3, 1/2, 2/5, and 1/3) compounds and also extended the search to other possible stoichiometries. All predicted structures have the common planar honeycomb character. Interestingly, many of the predicted structures possess direct band gaps with values that are in the optimal range for the solar light absorption, as well as broad adsorption bands, hinting at high solar conversion efficiency. More importantly, one can tune band gaps of $B_{x/2}N_{x/2}C_{1-x}$ to a desirable value by changing the concentration of carbon or BN. The dependence of the alloy band gap on concentration x can be roughly estimated by the equation $E_g(\text{eV})=5.1x^2 - 0.6x$. Although all the compounds show the trend of phase separation, phonon calculations on some

stoichiometries suggest that they are dynamically rather stable and are also thermally metastable to at least 1000 K in MD calculations. The findings of this work may open a new route to design materials with excellent optical and electronic properties.

Acknowledgements

References

1 A. Nag, K. Raidongia, K. P. Hembram, R. Datta, U. V. Waghmare and C. Rao, *ACS nano*, 2010, **4**, 1539-1544.

2 E. Almahmoud, I. Kornev and L. Bellaiche, *Phys. Rev. B*, 2010, **81**, 064105.

3 J. Zhou, Q. Wang, Q. Sun and P. Jena, *Phys. Rev. B*, 2010, **81**, 085442.

4 K. F. Mak, C. Lee, J. Hone, J. Shan and T. F. Heinz, *Phys. Rev. Lett.*, 2010, **105**, 136805.

5 Z. Yin, H. Li, H. Li, L. Jiang, Y. Shi, Y. Sun, G. Lu, Q. Zhang, X. Chen and H. Zhang, *ACS nano*, 2011, **6**, 74-80.

6 M. S. Hybertsen and S. G. Louie, *Phys. Rev. Lett.*, 1985, **55**, 1418.

7 D. Y. Kim, S. Stefanoski, O. O. Kurakevych and T. A. Strobel, *Nat. Mater.*, 2014, **14**, 169-173.

8 S. Botti, J. A. Flores-Livas, M. Amsler, S. Goedecker and M. A. Marques, *Phys. Rev. B*, 2012, **86**, 121204.

9 H. Xiang, B. Huang, E. Kan, S.-H. Wei and X. Gong, *Phys. Rev. Lett.*, 2013, **110**, 118702.

10 Q. Wang, B. Xu, J. Sun, H. Liu, Z. Zhao, D. Yu, C. Fan and J. He, *J. Am. Chem. Soc.*, 2014, **136**, 9826-9829.

11 W. Luo, Y. Ma, X. Gong and H. Xiang, *J. Am. Chem. Soc.*, 2014, **136**, 15992-15997.

12 L. L. Kazmerski, *J. Electron. Spectrosc. Relat. Phenom.*, 2006, **150**, 105-135.

13 Z. Zhang and W. Guo, *Phys. Rev. B*, 2008, **77**, 075403.

14 Z. Zhang, W. Guo and B. I. Yakobson, *Nanoscale*, 2013, **5**, 6381-6387.

15 L. Ci, L. Song, C. Jin, D. Jariwala, D. Wu, Y. Li, A. Srivastava, Z. Wang, K. Storr and L. Balicas, *Nat. Mater.*, 2010, **9**, 430-435.

16 Y. Gong, G. Shi, Z. Zhang, W. Zhou, J. Jung, W. Gao, L. Ma, Y. Yang, S. Yang and G. You, *Nat. Commun.*, 2014, **5**, 3193.

17 J. Lu, K. Zhang, X. F. Liu, H. Zhang, T. C. Sum, A. H. C. Neto and K. P. Loh, *Nat.Commun.*, 2013, **4**, 2681.

18 E. J. Kan, X. Wu, Z. Li, X. C. Zeng, J. Yang and J. Hou, *J. Chem. Phys.*, 2008, **129**, 084712.

19 P. Lu, Z. Zhang and W. Guo, *J. Phys. Chem. C*, 2011, **115**, 3572-3577.

20 Y. Liu, S. Bhowmick and B. I. Yakobson, *Nano letters*, 2011, **11**, 3113-3116.

21 S. Bhowmick, A. K. Singh and B. I. Yakobson, *J. Phys. Chem. C.*, 2011, **115**, 9889-9893.

22 Y. Wang, J. Lv, L. Zhu and Y. Ma, *Phys. Rev. B*, 2010, **82**, 094116.

23 Y. Wang, M. Miao, J. Lv, L. Zhu, K. Yin, H. Liu and Y. Ma, *J. Chem. Phys*, 2012, **137**, 224108.

24 J. M. Sanchez, F. Ducastelle and D. Gratias, *Physica A: Statistical Mechanics and its Applications*, 1984, **128**, 334-350.

25 H. Nozaki and S. Itoh, *J. Phys. Chem. Solids*, 1996, **57**, 41-49.

26 Z. Shi, A. Kutana and B. I. Yakobson, *J. Phys. Chem. Lett.*, 2014, **6**, 106.

27 X. Wu, J. Dai, Y. Zhao, Z. Zhuo, J. Yang and X. C. Zeng, *ACS nano*, 2012, **6**, 7443-7453.

28 S. Mohr, P. Pochet, M. Amsler, B. Schaefer, A. Sadeghi, L. Genovese and S. Goedecker, *Phys. Rev. B*, 2014, **89**, 041404.

29 Y. Kubota, K. Watanabe, O. Tsuda and T. Taniguchi, *Science*, 2007, **317**, 932-934.

30 J. Heyd and G. E. Scuseria, *J. Chem. Phys*, 2004, **120**, 7274.

31 A. Kutana, E. S. Penev and B. I. Yakobson, *Nanoscale*, 2014, **6**, 5820-5825.

32 W. Shockley and H. J. Queisser, *J. Appl. Phys.*, 1961, **32**, 510-519.

33 R. F. Service, *Science*, 2008, **319**, 718-720.

34 Y. Li, Y. Liao and Z. Chen, *Angew. Chem. Int. Ed.*, 2014, **53**, 7248-7252.

35 L. Zhu, H. wang, Y. Wang, J. Lv, Y. Ma, Q. Cui, Y. Ma and G. Zou, *Phys. Rev. Lett.*, 2011, **106**, 145501.

36 J. Lv, Y. Wang, L. Zhu and Y. Ma, *Phys. Rev. Lett.*, 2011, **106**, 015503.

37 Q. Li, D. Zhou, W. Zheng, Y. Ma and C. Chen, *Phys. Rev. Lett.*, 2013, **110**, 136403.

38 X. Wang, Y. Wang, M. Miao, X. Zhong, J. Lv, T. Cui, J. Li, L. Chen, C. J. Pickard and Y. Ma, *Phys. Rev. Lett.*, 2012, **109**, 175502.

39 P. E. Blochl, *Phys. Rev. B*, 1994, **50**, 17953.

40 G. Kresse and D. Joubert, *Phys. Rev. B*, 1999, **59**, 1758.

41 G. Kresse and J. Furthmüller, *Phys. Rev. B*, 1996, **54**, 11169.

42 J. P. Perdew, K. Burke and M. Ernzerhof, *Phys. Rev. Lett.*, 1996, **77**, 3865-3868.

43 J. Heyd, G. E. Scuseria and M. Ernzerhof, *J. Chem. Phys*, 2003, **118**, 8207.

44 A. Togo, F. Oba and I. Tanaka, *Phys. Rev. B*, 2008, **78**, 134106.

45 A. Van de Walle, M. Asta and G. Ceder, *Calphad*, 2002, **26**, 539-553.